Molecular Neurobiology (2019) 56:5626–5642
https://doi.org/10.1007/s12035-019-1474-9

Ginsenoside Rg1 Prevents Chemotherapy-Induced Cognitive Impairment: Associations with Microglia-Mediated Cytokines, Neuroinflammation, and Neuroplasticity

Dong-Dong Shi[1] · Yu-Hua Huang[2] · Cora Sau Wan Lai[2] · Celia M. Dong[3] · Leon C. Ho[3] · Xiao-Yang Li[2] · Ed X. Wu[3] · Qi Li[4] · Xiao-Min Wang[5] · Yong-Jun Chen[6] · Sookja Kim Chung[2] · Zhang-Jin Zhang[1]

Received: 6 September 2018 / Accepted: 10 January 2019 / Published online: 18 January 2019

Abstract

Chemotherapy-induced cognitive impairment, also known as "chemobrain," is a common side effect. The purpose of this study was to examine whether ginsenoside Rg1, a ginseng-derived compound, could prevent chemobrain and its underlying mechanisms. A mouse model of chemobrain was developed with three injections of docetaxel, adriamycin, and cyclophosphamide (DAC) in combination at a 2-day interval. Rg1 (5 and 10 mg/kg daily) was given 1 week prior to DAC regimen for 3 weeks. An amount of 10 mg/kg Rg1 significantly improved chemobrain-like behavior in water maze test. In vivo neuroimaging revealed that Rg1 co-treatment reversed DAC-induced decreases in prefrontal and hippocampal neuronal activity and ameliorated cortical neuronal dendritic spine elimination. It normalized DAC-caused abnormalities in the expression of multiple neuroplasticity biomarkers in the two brain regions. Rg1 suppressed DAC-induced elevation of the proinflammatory cytokines tumor necrosis factor-α (TNF-α) and interleukin-6 (IL-6), but increased levels of the anti-inflammatory cytokines IL-4 and IL-10 in multiple sera and brain tissues. Rg1 also modulated cytokine mediators and inhibited DAC-induced microglial polarization from M2 to M1 phenotypes. In in vitro experiments, while impaired viability of PC12 neuroblastic cells and hyperactivation of BV-2 microglial cells, a model of neuroinflammation, were observed in the presence of DAC, Rg1 co-treatment strikingly reduced DAC's neurotoxic effects and neuroinflammatory response. These results indicate that Rg1 exerts its anti-chemobrain effect in an association with the inhibition of neuroinflammation by modulating microglia-mediated cytokines and the related upstream mediators, protecting neuronal activity and promoting neuroplasticity in particular brain regions associated with cognition processing.

Keywords Ginsenoside Rg1 · Chemobrain · Cytokines · Neuroinflammation · Neuroplasticity · In vivo neuroimaging

Electronic supplementary material The online version of this article (https://doi.org/10.1007/s12035-019-1474-9) contains supplementary material, which is available to authorized users.

✉ Zhang-Jin Zhang
zhangzj@hku.hk

[1] School of Chinese Medicine, LKS Faculty of Medicine, The University of Hong Kong, 10 Sassoon Road, Pokfulam, Hong Kong, China

[2] School of Biomedical Sciences, State Key Laboratory of Pharmaceutical Biotechnology, LKS Faculty of Medicine, The University of Hong Kong, Hong Kong, China

[3] Laboratory of Biomedical Imaging and Signal Processing, Department of Electrical and Electronic Engineering, The University of Hong Kong, Hong Kong, China

[4] Department of Psychiatry, State Key Laboratory of Cognitive and Brain Sciences, HKU-SIRI, The University of Hong Kong, Hong Kong, China

[5] Department of Anesthesiology, LKS Faculty of Medicine, The University of Hong Kong, Hong Kong, China

[6] South China Research Center for Acupuncture and Moxibustion, Guangzhou University of Chinese Medicine, Guangzhou 510006, China

Introduction

Chemotherapy-induced cognitive impairment, also known as "chemobrain," is often observed in cancer patients during and even post-chemotherapy. It is particularly apparent in breast cancer patients with a prevalence of 69–78% [1, 2]. Chemobrain mainly manifests as forgetfulness, trouble with multi-tasking and executing tasks, difficulties in learning and memory, decreased processing speed, and poor attention span [3]. It has become a growing healthcare issue with extensive use of chemotherapy and tremendous improvement in survival rate of cancer patients [4]. However, there is a dearth of effective interventions for the management of chemobrain. A search of novel anti-chemobrain treatment is therefore highly desired.

Cytokine dysregulation is thought to be a primary pathology of chemobrain [5]. The peripheral circulating cytokines released from tumor and damaged cells and tissues during chemotherapy can cross the blood–brain barrier (BBB) and recruit microglia to overproduce proinflammatory cytokines, such as tumor necrosis factor α (TNF-α) and interleukin-6 (IL-6), and suppress antiinflammatory cytokines, such as IL-4 and IL-10 [5]. Meanwhile, a small amount of chemotherapeutic drugs can cross the BBB and enter the brain, directly triggering microglia to release cytokines in response to chemotherapeutic insult [5]. Microglia-mediated neuroinflammation plays a key role in the pathogenesis of chemobrain, as it could impair neuroprotective and neuroplasticity mechanisms that are closely associated with cognitive function [5–7]. Our recent study has demonstrated an association of chemobrain with brain cytokine dysfunction and impaired neuroplasticity [8]. This has led to the supposition that agents that have cytokine-modulating, neuroprotective, and anti-inflammatory effects may have the preventive potential against chemobrain.

Ginsenoside Rg1, a natural compound derived from ginseng, has been extensively investigated over the past two decades. Rg1 has anti-inflammatory, antioxidant, and anti-apoptotic activities [9, 10]. It has been shown to improve cognitive performance and restore neuroplasticity-associated molecular and electrophysiological functions in the hippocampus of a mouse model of Alzheimer's disease [11]. Rg1 can modulate various cytokines and reduce neuroinflammation and neural damage [12]. These studies have led to the hypothesis that Rg1 could attenuate chemotherapy-induced cognitive deterioration via its modulation of microglia-mediated cytokines, inhibition of neuroinflammation, and protection of neuroplasticity in the prefrontal cortex and hippocampus, the two brain regions closely associated with cognitive processing.

To test this hypothesis, behavioral, in vivo neuroimaging, and cytokine effects of Rg1 were examined in a mouse model of chemobrain which was produced with three injections of docetaxel, adriamycin, and cyclophosphamide (DAC) in combination, a commonly used chemotherapy regimen [13]. The expression of cytokine mediators, biomarkers for neuroplasticity, astrocyte activation, and microglial polarization were also examined in mice's brain regions and in the two cell lines, BV-2 microglial cells, a model of neuroinflammation, and PC12 neuroblastic cells were additionally used to examine microglial and neuroprotective effects.

Materials and Methods

Animals

The animal experiment protocol was approved by the Committee on the Use of Live Animal in Teaching and Research (CULATR 3531-14 and 3267-14) of LKS Faculty of Medicine of the University of Hong Kong. Female C57/BL6J mice (Charles River Laboratory, USA) weighing 18–20 g were used for most experiments. Thy1-YFP H-line transgenic mice were used in in vivo transcranial two-photon microscopy. All animals were housed in clear plastic cages and maintained on a 12 light/dark cycle at 23 °C with water and food available ad libitum.

Treatment and Experimental Procedures

The treatment schedule is shown in Table 1. The model of chemobrain was established with three intraperitoneal (i.p.) injections of 10/10/40 mg/kg DAC at a 2-day interval within 1 week as previously reported [8]. Vehicle (0.9% saline solution, DAC group) or Rg1 with a dose of 5 mg/kg (Rg1 5 mg group) or 10 mg/kg (Rg1 10 group) per day was co-administered (i.p.) 1 week prior to DAC regimen for 3 weeks. An additional group of mice treated with vehicle for 3 weeks in parallel with other three groups was included as control group. Following the completion of treatment, animals were tested in behavioral paradigms and in vivo neuroimaging, and then killed to collect blood and brain tissues.

Behavioral Test

Following the completion of treatment, animals were tested in an open field apparatus to detect their anxiety levels and locomotor activity, and then in a Morris water maze to examine their cognitive performance. All testing was conducted between 09:00 and 12:00, videotaped, and analyzed with video tracking software (Ethovision, Noldus, Netherlands). The order of testing was random.

Open Field Test Open field test was applied to determine whether the DAC and Rg1 treatment could affect anxiety and locomotor abilities. The open field apparatus was a 40 × 40 × 60 cm Plexiglas arena with clear walls, a white floor, and

Table 1 Experimental procedure

C57/BL6J mice	Day	1–7	8	9, 10	11	12, 13	14	15–21	22	23	24–29	30	31	32
	Control	S	S	S	S	S	S	S	OFT	Rest	WMT	Rest	MEMRI	Tissue collection
	DAC	S	DAC	Rg1	DAC	S	DAC	S						
	Rg1 5	Rg1	Rg1 + DAC	Rg1	Rg1 + DAC	Rg1	Rg1 + DAC	Rg1						
	Rg1 10	Rg1	Rg1 + DAC	Rg1	Rg1 + DAC	Rg1	Rg1 + DAC	Rg1						
Thy1-YFP mice	Day	1–7	8	9, 10	11	12, 13	14	15–21	22	23	24–25	26		27
	Control	S	S	S	S	S	S	S	Rest	Two-photon initial imaging	Rest	Two-photon reimaging		Tissue collection
	DAC	S	DAC	Rg1	DAC	S	DAC	S						
	Rg1 10	Rg1	Rg1 + DAC	Rg1	Rg1 + DAC	Rg1	Rg1 + DAC	Rg1						

DAC, docetaxel + adriamycin + cyclophosphamide; S, saline; OPT, open field test; WMT, water maze test; MEMRI, manganese-enhanced magnetic resonance imaging; Rg1 5, 5 mg/kg ginsenoside Rg1; Rg1 10, 10 mg/kg ginsenoside Rg1

a 25 × 25 cm central zone. The testing was conducted in dimly lit conditions without experimenters' presence. The total distance and velocity moved and the frequency of transfer between the central and surrounding zones were recorded over a 10-min test period. The apparatus was cleaned with 75% alcohol between tests.

Morris Water Maze Test This test was used to evaluate the mice's spatial learning and memory abilities. Our experiment consisted of five successive training trials and a probe test. Briefly, a white circular tank (120 cm in diameter, 50 cm in height) filled with water (22 ± 2 °C) was circled by a black cloth curtain. Four distal landmarks of different shape and color were present around the tank during training days. The mice were trained to find a hidden hyaline platform (10 cm in diameter, 24 cm in height) that was submerged 1 cm below the surface of the water and situated in the same location on the training days. Each mouse underwent four successive training trials per day for 5 days, with 15-min intervals between trials.

The mouse was gently released onto the water at the desired start position in the maze, facing the tank wall. The sequence of starting points was different each day to help the mice gain spatial memory of the area. Each mouse's movement trajectory in the maze was recorded with the video tracking software. The training trial ended if the mouse reached the hidden platform and stayed on the platform for at least 10 s, or could not find the platform within 60 s. Those who could not find the platform within the defined period were guided to the platform and allowed to stay there for 15 s. The escape latency to the platform was recorded for each training trial.

A probe test was carried out 24 h after the last training trial. The platform was removed, and the mouse was placed in a new start position to ensure it used its spatial memory, rather than following a specific swim pathway. The mouse was allowed to swim freely for 60 s. The duration spent in the targeted quadrant and the other three quadrants and the frequency into the targeted quadrant were obtained as variables of learning and memory abilities.

In Vivo Neuroimaging

Manganese-Enhanced Magnetic Resonance Imaging (MEMRI) MEMRI was used to examine prefrontal and hippocampal neuronal activity as previously reported [8]. Briefly, mice were injected (i.p.) with $MnCl_2$ (45 mg/kg) 4 h before MEMRI, with water and food available ad libitum. Mice were anesthetized with isoflurane (2.5% for induction and 1.0% for maintenance). They were placed on a holder in the prone position with facemask. During the course of MRI scan, mice were kept warm using a warming system (Bruker BioSpin MRI GmbH). Respiratory rate was continuously monitored using MRI-compatible sensors (SA instruments) and kept in a range of 90–110 times per minute.

Scan was conducted on a 7-Tesla MRI scanner with maximum gradient of 360 mT/m (70/16 PharmaScan; Bruker Biosin GmbH, Germany). Standard multislice coronal images were obtained with FOV = 2.5 × 2.5 cm^2, slice thickness = 0.5 mm, matrix = 256 × 256, and 15 continuous slices. T1-weighted images were acquired by a RARE sequence with TR = 1366.7 ms, TE_{eff} = 7.5 ms, RARE factor = 4, and NEX = 6. The signal intensity was calculated as the ratio between the mean signal in hippocampal or prefrontal regions and the mean signal of the adjacent corpus callosum using Image J software (Wayne Rasband, NIH, USA). After the completion of the imaging, sera were collected via cardiac puncture and brains were removed for cytokine measurement (see below).

In Vivo Transcranial Two-Photon Imaging In vivo transcranial two-photon microscopy is a useful tool for the investigation of neuroplasticity by longitudinal observation of the formation and elimination of dendritic spines of cortical neurons in living animals [14, 15]. This separate experiment was conducted in Thy1-YFP H-line transgenic mice that expressed yellow fluorescent proteins in pyramidal neurons located in cortical layer V. The experimental procedure was described in our previous study [16]. Briefly, each mouse was anesthetized with an intraperitoneal injection of 120 mg/kg ketamine and 18 mg/kg xylazine and its head was attached to a head-holder to prepare a thinned-skull window using a high-speed microdrill. A round window of about 0.8 mm and a skull thickness of about 20 μm was created at the medial prefrontal cortex.

The initial imaging and re-imaging were conducted at a 3-day interval. A ×25, NA 1.05 water-immersion objective (Olympus) and a 920-nm two-photon laser were used to acquire the images. High-magnification images were scanned in a Z-stack manner (thickness, 80 to 120 μm; layer interval, 0.75 μm). For re-imaging of the same region, the thinned regions were identified based on the map of the brain vasculature, and microsurgical blades were used to further thin the region of interest until a clear image could be obtained. The imaging region was 216 × 216 μm, and its center was located at the frontal association cortex (+ 2.8 mm Bregma, + 1.0 mm midline). The captured images of dendritic spines were analyzed using Image J software (Wayne Rasband, NIH, USA).

The number of eliminated and newly formed spines and filopodia were counted from nine imaged areas chosen at random. The percentages of the types of spines and filopodia were calculated. The analysts were blinded to the animal treatment. After imaging, sera and brain tissues were collected for further analysis (see the following).

Cytokine Measurement

Following the completion of in vivo imaging, both C57/BL6J and Thy1-YFP transgenic mice were further used for cytokine measurement. Then 0.5–0.6 ml blood was collected via cardiac puncture; serum was separated immediately and stored at − 80 °C for cytokine measurement. The mice then received cardiac reperfusion and the whole brains were collected. The hippocampus and prefrontal cortex were dissected from half of the whole brains (n = 4–5). For the measurement, brain tissues were prepared according to the protocol provided in the enzyme-linked immunosorbent assay (ELISA) kit (eBioscience, Thermo Fisher). Briefly, approximately 10 mg tissues were homogenized in 100 μl of 0.1 M PBS containing 1% phenylmethanesulfonyl fluoride (PMSF; Sigma-Aldrich, USA) and 1% protein inhibitor (Sigma-Aldrich, USA) on ice for 30 min. The homogenate was then centrifuged at 20,000×g at 4 °C for 20 min. The supernatant was separated for ELISA analysis. The level of four cytokines, IL-4, Il-6, IL-10, and TNF-α, in serum and brain was measured using ELISA kit (eBioscience, Thermo Fisher) as previously described. The absorbance of each well for cytokine reactions was measured at 450 nm. The concentrations of cytokines were calculated from standard curves that were constructed with the four-parameter logistic curve fitting model by plotting the mean absorbance obtained for each reference standard against each cytokine concentration.

Immunohistological Examination

Tissue Preparations Immunohistological examination was carried out to examine the effects of Rg1 on immunohistological profiles of astrocytes and M1/M2 phenotypes of microglia in the brain and BV2 cells. For this purpose, part of mice were anesthetized with ketamine/xylazine (120/18 mg/kg) and subsequently perfused with 0.9% saline for 5 min, followed by 4% paraformaldehyde (PFA) in phosphate buffer. Brains were removed, fixed in 4% PFA overnight, and transferred into the 30% sucrose in PBS until sinking to the bottom of the 50-ml tube. Coronary sections at a thickness of 15 μm were cut on a freezing vibratome for immunodetection. For BV2 cells, glass slides onto which BV2 cells adhered were carefully taken out from the bottom of the culture plates, fixed in 4% PFA for 15 min, and permeabilized by incubating with 2 ml 0.3% Triton X-100 in PBS for 15 min on ice.

Immunohistochemistry Brain sections were pre-treated with hydrogen peroxidase (3% H_2O_2 in methanol) to block endogenous peroxidase activity for 15 min, followed by the addition of 1% BSA/0.5% Triton X-100 for 60 min to reduce non-specific hydrophobic interactions between the primary antibodies and the tissue. Sections were then incubated with primary antibody mouse anti-glial fibrillary acidic protein (GFAP) (1:200; Cell Signaling Technology) at 4 °C overnight, rinsed with PBS for three times, and incubated with biotinylated secondary antibody with avidin–biotin–HRP (goat anti-mouse, 1:200; Abcam) for 1 h at room temperature. The sections were then treated with 3,3′-diaminobenzidine (DAB)

(Dako) for 10 min. Histological images were captured on an Olympus BX43 microscope. Percent of $GFAP^+$ area was calculated from five imaged areas under ×20 field randomly chosen from each brain region (prefrontal cortex, hippocampal DG, CA1, and CA3) using ImageJ software.

Immunofluorescence Brain sections and BV2 cells were blocked for 60 min and then incubated at 4 °C overnight in the following primary antibodies as microglia biomarkers: goat anti-ionized calcium binding adaptor molecule 1 (Iba-1, 1:500; Abcam), rabbit anti-Arginase 1 (Arg-1, 1:200; Cell Signaling Technology), nuclear factor kappa-light-chain-enhancer of activated B cells (p65-NFκB, 1:200; Cell Signaling Technology), and mouse anti-IL-6 (1:200; Abcam). Tissues were then incubated respectively with the fluorescent-dye-conjugated secondary antibodies (Abcam), DyLight 594-conjugate donkey anti-goat, DyLight 488-conjugate donkey anti-rabbit, and DyLight 594-conjugate donkey anti-rabbit at a concentration of 1:200 for 1 h at room temperature. Slides were co-stained with 4′,6-diamidino-2-phenylindole (DAPI), a nuclear and chromosome counterstain, for 15 min. Images were captured using a Zeiss confocal microscope (Zeiss, LSM800, Germany). Percent of $Iba\text{-}1^+$, Arg^+, and $IL\text{-}6^+$ area were calculated from five imaged areas under ×20 field randomly chosen from each brain region (prefrontal cortex, hippocampal DG, CA1, and CA3) or cultured BV20 microglial cells using ImageJ software chosen at random using ImageJ software.

Treatment and Assays of Cultured Cells

BV-2 Microglial Cells BV-2 murine microglial cells have been widely used as a valid model to investigate neuroinflammation-related diseases [17]. In this study, BV-2 cells (ATCC, Rockville, MD, USA) were cultured in Dulbecco's modified Eagle's medium (DMEM; Thermo Scientific, Waltham, MA, USA) supplemented with 10% FBS, 1% penicillin (100 IU/ml), and streptomycin (100 μg/ml) under a humidified atmosphere containing 5% CO_2 and 95% air at 30 °C. The cells were seeded into six-well plates (34.8 mm in diameter and 9.5 cm^2 in area) at a density of 5×10^5 per well. After 24 h of incubation, those that grew well were transplanted into new six-well plates containing glass slides in the bottom and incubated for additional 24 h. The cells were pre-treated with the absence or presence of Rg1 (20 μM and 40 μM) 2 h before exposure to 1/1/4 μg/ml DAC or 1 μg/ml lipopolysaccharides (LPS), an endotoxin, for 24 h. The cells were then harvested for immunofluorescence and Western blot analysis. The media were collected separately for the treatment of PC12 neuroblastic cells (see below).

PC12 Neuroblastic Cells PC12 neuroblastic cells (ATCC, Rockville, MD, USA) were used to examine the protective effects of Rg1 against microglia-mediated neuronal viability. The cells were cultured as the same as described for BV-2 cells. PC12 cells were seeded in 96-well plates and treated with the media separately collected from the culture of BV2 microglial cells for 24 h. After that, cell viability was examined using an MTT assay. Briefly, 15 μl MTT (5 mg/ml in PBS) was added into each well and the plates were incubated at 37 °C for 4 h in darkness. The supernatant was aspirated and 150 μl of dimethyl sulfoxide (DMSO) was added into each well. After 15-min shaking, the reaction products were quantified by measuring absorbance at 495 by multi-plate reader (Model 680; Bio-Rad Laboratories Inc., USA).

Western Blot Analysis

Western blot analysis was performed to examine the expression of cytokine mediators, biomarkers for microglia-mediated neuroinflammation, and neuroplasticity in the prefrontal cortex and hippocampus.

Both brain tissue and cell proteins were extracted by RIPA buffer (Sigma-Aldrich, USA) containing 1% phenylmethanesulfonyl fluoride (PMSF; Sigma-Aldrich, USA) and 1% protein inhibitor (PI; Sigma-Aldrich, USA). The protein concentrations were determined using Bradford protein assay with Coomassie brilliant blue G-250 (Bio-Rad Laboratories Inc., USA). Proteins were separated by a 10% SDS-PAGE gel and transferred electrophoretically onto nitrocellulose membranes (0.45 μm; Bio Basic, Inc.).

Immunodetection was performed with the primary antibodies against GFAP (Cell Signaling Technology), Iba1 (Abcam), Arg-1 (Cell Signaling Technology), IL-6 (Abcam), and TNF-α (Santa Cruz Biotechnology) for microglia-mediated neuroinflammation biomarkers; brain peroxisome proliferator activated receptor gamma (PPARγ; Invitrogen), p65-NFκB (Cell Signaling Technology), and phosphorylation of NFκB (p-p65-NFκB; Cell Signaling Technology) for cytokine mediators; γ-aminobutyric acid receptor type A ($GABA_AR$; Santa Cruz Biotechnology), *N*-methyl-D-aspartate receptor subunit 1 (NMDAR1; Santa Cruz Biotechnology), brain-derived neurotrophic factor (BDNF; Santa Cruz Biotechnology), calmodulin-dependent protein kinase II (CaMK-II; Santa Cruz Biotechnology), phospho-CaMKII (p-CaMKII; Santa Cruz Biotechnology), and tropomyosin receptor kinase B (TrkB; Santa Cruz Biotechnology) for neuroplasticity biomarkers. The antibody against glyceraldehyde 3-phosphate dehydrogenase (GAPDH; Invitrogen) was included as internal control. All immunoreactions were conducted with the primary antibodies at a final concentration of 1:2000 for 4 h at 4 °C. The chemiluminescence was detected using ECL detection kits (GE Healthcare, UK). The intensity of protein bands was quantified by scanning densitometry with Quantity One 4.5.0 software.

Statistical Analysis

Two-way analysis of variance (ANOVA) was used to detect statistical differences among the four groups in changes in body weight over time and escape latency to the platform during water maze training trials. Other behavioral, in vivo neuroimaging, cytokine, and immunodetection analyses were examined using one-way ANOVA. If main effects reached significant level, Student–Newman–Keuls method was further used as post hoc comparisons to detect between-group differences. GraphPad Prism 7.0 software was used for statistical analysis. Data are expressed mean ± standard error of the mean (SEM). Statistical significance was defined as $P < 0.05$ with a two-sided test.

Results

Behavioral Effects on Anxiety, Locomotor, and Cognitive Performance

In open field test, there were no differences among the four groups in number of entry into the center area, time stayed in the central zone, and movement velocity ($F_{3,32} \leq 0.080$, $P \geq 0.971$) (Fig. S1).

Training trials of water maze test showed that animals had no spatial bias and differences in basic swim speed (data not shown). Two-way ANOVA revealed marked significant main effects of group ($F_{3,760} = 18.170$, $P < 0.0001$) and training days ($F_{4,760} = 134.000$, $P < 0.0001$) on the escape latency to the platform. Post hoc comparisons showed that the latency of the DAC group was strikingly longer than that of controls at trials 4 and 5 ($P \leq 0.047$). Ten-milligram Rg1 co-treatment markedly reduced the latency to the hidden platform at trials 2, 4, and 5 compared to the DAC group ($P \leq 0.001$) (Fig. 1a, b). An amount of 5 mg/kg Rg1 did not produce significant effects in training trials.

In the probe test, significant group effects were observed on duration spent in ($F_{3,36} = 11.190$, $P < 0.0001$) and number of entries into the targeted quadrant ($F_{3,36} = 5.434$, $P = 0.004$) (Fig. 1c, d), but not on distance moved ($F_{3,36} = 0.985$, $P = 0.411$) (Fig. 1e). There were no differences in duration spent in other three quadrants (Fig. 1c). The duration spent in and number of entries into the targeted quadrant were significantly greater in mice co-treated with 10 mg/kg Rg1 than in the DAC group ($P \leq 0.014$). The two variables of the DAC group were markedly less than those of controls ($P \leq 0.012$). Moreover, 5 mg/kg Rg1 had no effects in the probe test.

Effects on MEMRI-Measured Prefrontal and Hippocampal Neuronal Activity

Based on the results of water maze test, mice co-treated with 10 mg/kg Rg1 with the DAC group and controls

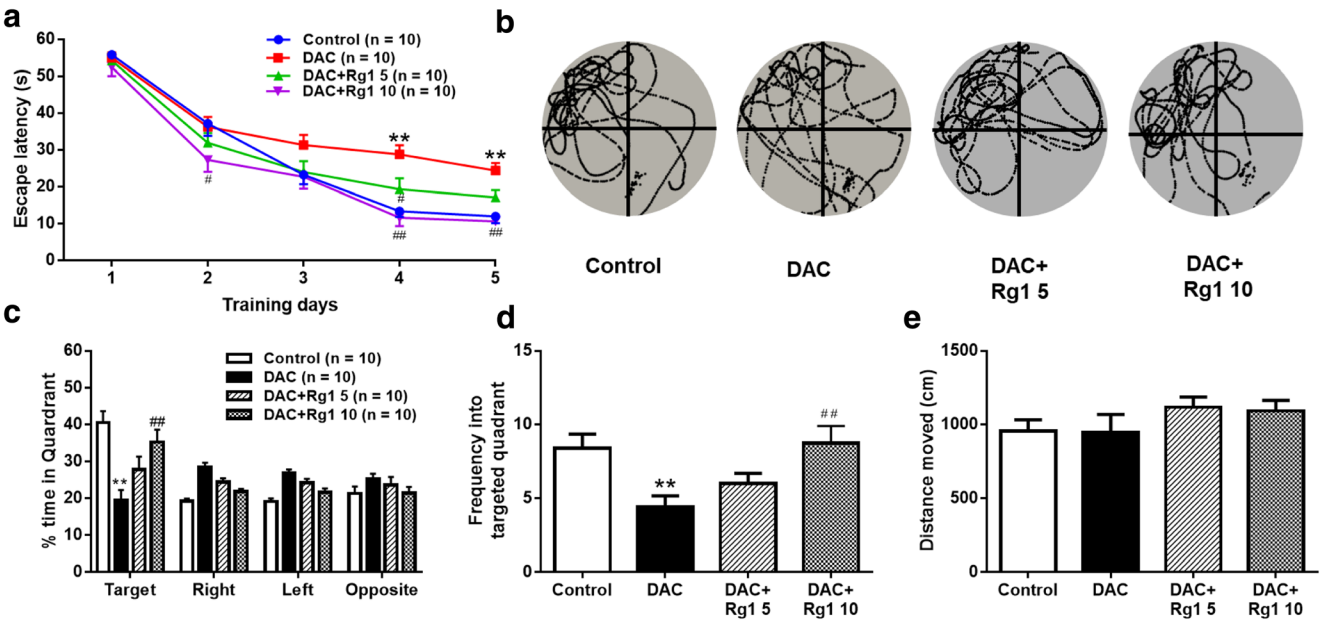

Fig. 1 Effects of rg1 in DAC-treated mice in water maze test. Escape latency to hidden platform in training trials (**a**), representative swimming path (**b**), duration stay in four quadrants (**c**), frequency into targeted quadrant (**d**), and distance moved (**e**) during probe test were recorded and analyzed. Data are expressed as mean ± SEM: $^{*}P < 0.05$, $^{**}P < 0.01$, and $^{***}P < 0.001$ compared to control; $^{\#}P < 0.05$, $^{\#\#}P < 0.01$, and $^{\#\#\#}P < 0.001$ compared to DAC group

were chosen for MEMRI scan. Significant group effects on MEMRI signal intensity were present in the prefrontal cortex ($F_{2,12} = 12.700$, $P = 0.001$), whole hippocampus ($F_{2,12} = 10.340$, $P = 0.003$), and its three subregions, the dentate gyrus ($F_{2,12} = 8.783$, $P = 0.004$), CA1 ($F_{2,12} = 7.587$, $P = 0.007$), and CA3 ($F_{2,12} = 13.420$, $P = 0.001$) (Fig. 2). The signal intensity was markedly decreased in all brain areas examined of the DAC group as compared to controls ($P \leq 0.004$) which has been reported in our previous study [8], but significantly increased in all the five brain areas of mice co-treated with Rg1 compared to the DAC group ($P \leq 0.020$).

Effects on Two-Photon-Measured Cortical Neuronal Dendritic Spine Plasticity

In vivo transcranial two-photon imaging in the transgenic mice showed significant group effects on dendritic spine elimination rate ($F_{2,10} = 17.050$, $P = 0.001$) and net loss of spines ($F_{2,10} = 40.700$, $P < 0.0001$) (Fig. 3). The DAC group had a striking increase in dendritic spine elimination rate ($P < 0.0001$) and a significant net loss of spines ($P < 0.0001$) in the frontal association cortical neurons compared with controls. Both variables were reversed by co-treatment with 10 mg/kg Rg1 ($P < 0.0001$). The spine density ratio was

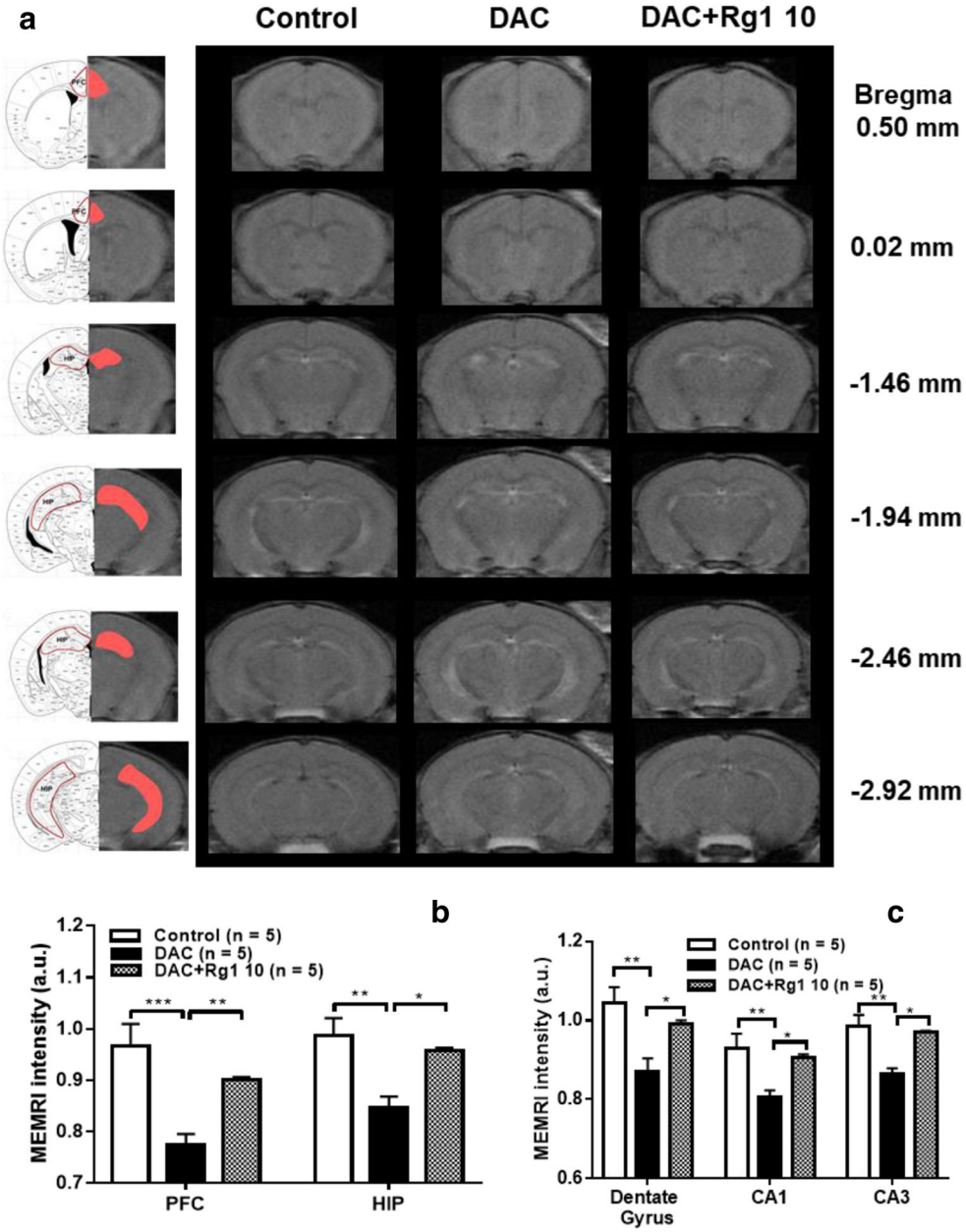

Fig. 2 Effects of 10 mg/kg Rg1 on MEMRI signal intensity in the prefrontal cortex (PFC), hippocampus (HIP), and its subregions (CA1, CA3, and dentate gyrus) in DAC-treated mice. Coronal brain sections of MEMRI scanning and the brain regions detected are shown (**a**). MEMRI data of control and DAC group has been used in our previous study [8]. Data are expressed as mean ± SEM (**b**, **c**): $^{*}P < 0.05$, $^{**}P < 0.01$, and $^{***}P < 0.001$

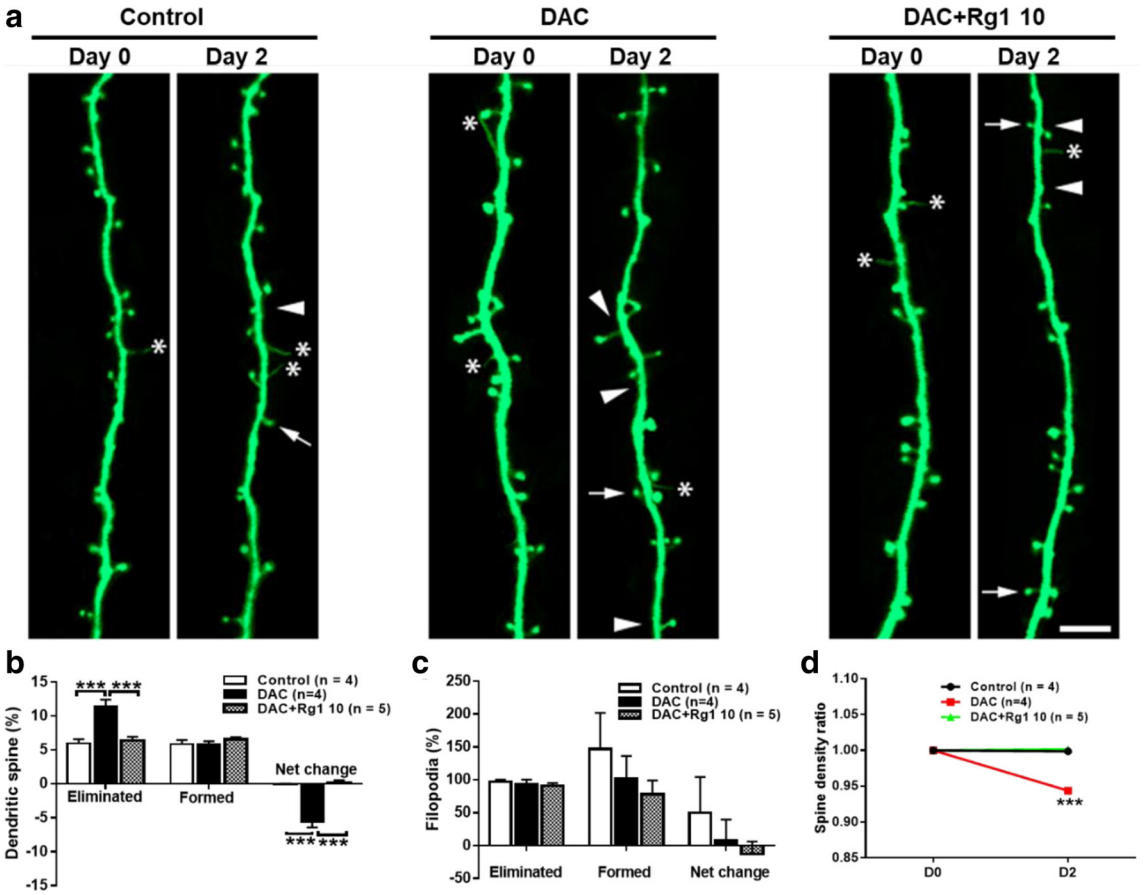

Fig. 3 The effects of 10 mg/kg Rg1 in DAC-treated mice on two-photon microscopy-detected dendritic spines of the prefrontal cortical neurons in Thy1-YFP H-line transgenic mice (**a**). Percentages of eliminated, newly formed, and net change in spines (**b**), filopodia (**c**), and spine density (**d**). Data are expressed as mean ± SEM and analyzed using one-way ANOVA: ***$P < 0.001$. Newly formed, eliminated spines, and filopodia are indicated with arrows, arrowheads, and stars, respectively, in (**a**) (scale bar = 5 μm)

remarkably lower in the DAC group ($P < 0.0001$) than controls, but not different between the Rg1 group and controls. Both DAC and Rg1 had no effects on filopodia.

Effects on Neuroplasticity Biomarkers

The expression of six neuroplasticity biomarkers in the two strains of mice was analyzed with Western blot in the prefrontal cortex and hippocampus of controls, DAC, and 10 mg/kg Rg1 groups (Fig. 4). These six biomarkers are $GABA_AR$, NMDAR1, and its downstream signaling proteins, CaMKII, p-CaMKII, BDNF, and TrkB. In wild-type mice, one-way ANOVA revealed marked differences among the three groups in all the six biomarkers of the two brain regions ($F_{2,12} \geq 59.860$, $P \leq 0.011$). The DAC group had strikingly lower levels of $GABA_AR$, NMDAR1, CaMKII, BDNF, and TrkB, but remarkably higher levels of p-CaMKII in the two brain regions compared to controls ($P < 0.0001$). Rg1 co-treatment partially or completely reversed all these variables to controls' levels ($P \leq 0.005$). In the transgenic mice (Fig. S2), significant group effects were present in all the six hippocampal biomarkers, prefrontal NMDAR1, and BDNF ($F_{2,12} \geq 17.510$, $P \leq 0.029$). The effects of DAC and Rg1 were similar to those observed in wild mice on the six hippocampal biomarkers ($P \leq 0.006$), prefrontal NMDAR1, and BDNF expression ($P \leq 0.033$).

Effects on Serum and Brain Cytokine Levels

In C57/BL6J mice, TNF-α, IL-6, IL-10, and IL-4 levels were measured in serum, whole brain, prefrontal cortex, and hippocampus (Fig. 5). Significant group effects were present on TNF-α, IL-10, and IL-4 levels in the four tissues examined ($F_{2,48} \geq 160.000$, $P < 0.0001$), IL-6 level in the whole brain ($F_{2,12} = 53.780$, $P < 0.0001$) and hippocampus ($F_{2,48} = 64.780$, $P < 0.0001$). The DAC group had strikingly higher levels of TNF-α in all the four tissues tested ($P \leq 0.001$), IL-6 in the whole brain and hippocampus ($P < 0.0001$), but markedly lower levels of IL-10 and IL-4 in the four tissues ($P \leq 0.001$) than controls. Co-treatment with 5 mg/kg Rg1 reversed DAC-induced abnormal levels of serum, prefrontal, and hippocampal TNF-α; whole brain and hippocampal IL-6; whole brain and prefrontal IL-4; and prefrontal IL-6 ($P \leq 0.019$). Co-treatment with 10 mg/kg Rg1 reversed all the DAC-induced

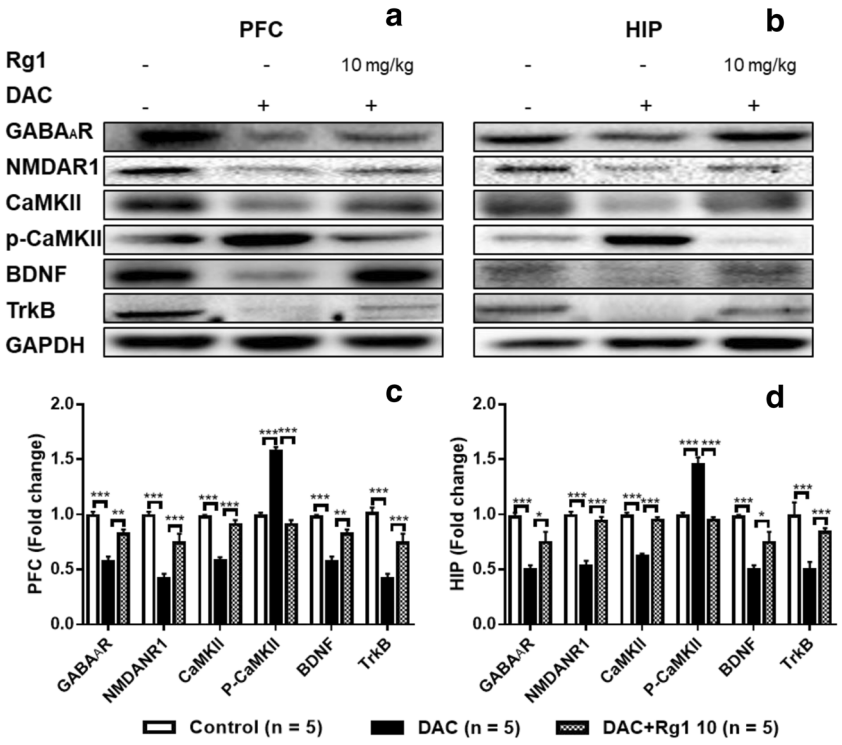

Fig. 4 Western blot analysis of $GABA_AR$, NMDAR1, CaMKII, p-CaMKII, BDNF, and TrkB in the prefrontal cortex (**a**) and hippocampus (**b**) in C57 wild-type mice. Data are expressed as mean ± SEM, where $*P < 0.05$, $**P < 0.01$, and $***P < 0.001$

abnormal cytokine levels, with significant differences from the DAC groups ($P \leq 0.001$).

In Thy1-YFP H-line transgenic mice, the four cytokine levels were measured in serum, prefrontal cortex, and hippocampus. The results were consistent with wild-type mice (Fig. S3). Significant group effects were observed on TNF-α in all the three tissues ($F_{2,10} \geq 246.500$, $P < 0.0001$), IL-6 in the prefrontal cortex ($F_{2,10} = 5.236$, $P = 0.028$) and hippocampus ($F_{2,10} = 242.800$, $P = 0.0001$), IL-4 in the two brain regions ($F_{2,10} \geq 13.180$, $P \leq 0.002$), and IL-10 in serum ($F_{2,10} = 4.230$, $P < 0.047$) and hippocampus ($F_{2,10} = 7.583$, $P = 0.010$). The DAC group displayed significantly higher levels of TNF-α in all the three tissues examined ($P \leq 0.015$) and IL-6 in the two brain tissues ($P < 0.0001$), but prominently lower levels of IL-4 in the two brain tissues ($P \leq 0.001$) and IL-10 in serum and hippocampus ($P \leq 0.028$). Co-treatment with 10 mg/kg Rg1 partially and even completely reversed all the DAC-caused abnormal cytokine levels, with significant differences from the DAC groups ($P \leq 0.039$).

Effects on Cytokine Mediators in the Brain Tissues

The four cytokine mediators of PPARγ/NF-κB signaling pathways, PPARγ, p65, and p-p65 were detected in the prefrontal cortex and hippocampus of the two strains of mice (Fig. 5). In wild-type mice, significant group effects were observed in all the four biomarkers of the two brain regions ($F_{2,12} \geq 4.200$, $P \leq 0.011$), except prefrontal p65 expression. DAC strikingly decreased the expression of prefrontal PPARγ, hippocampal PPARγ, and p65 ($P < 0.0001$), but remarkably increased the expression of p-p65 in both brain regions ($P < 0.050$) compared with controls. Co-treatment with 10 mg/kg Rg1 reversed these DAC-induced altered variables to controls' levels ($P \leq 0.032$). In the transgenic mice, one-way ANOVA showed significant effects of group on PPARγ and p-p65 in both brain regions ($F_{2,12} \geq 8.047$, $P \leq 0.021$) (Fig. S4). The effects of DAC and Rg1 on the expression of the three variables were similar to those observed in wild-type mice ($P \leq 0.050$).

Effects on GFAP Immunoreactivity in Brain Tissues

Immunohistochemical analysis was used to examine GFAP immunoreactivity in the prefrontal cortex and the three hippocampal subregions, dentate gyrus, CA1, and CA3 (Fig. 6). Direct microscopic observations revealed apparently higher density GFAP-positive astrocytes with extensively ramified processes over all the four brain regions examined of the DAC group compared to controls (Fig. 6a). The quantitative analysis showed significant group effects on GFAP-immunoreactive area in the four brain regions ($F_{2,12} \geq 3.832$, $P \leq 0.042$). The GFAP area of the DAC group was prominently greater than that of controls and mice co-treated with 10 mg/kg Rg1 ($P \leq 0.033$), but not different between the latter two groups (Fig. 6b).

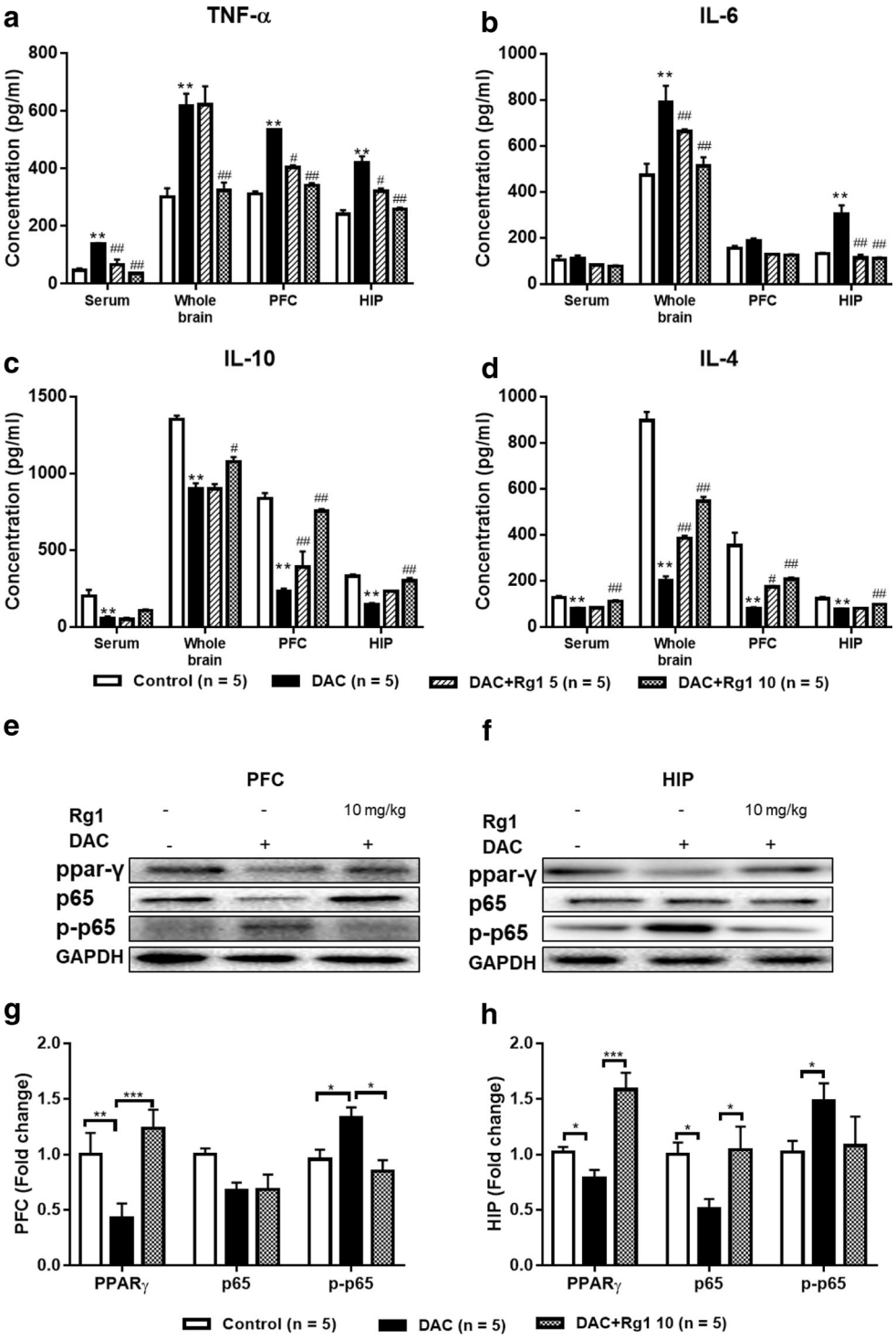

Fig. 5 Effects of Rg1 on TNF-α (**a**), IL-6 (**b**), IL-10 (**c**), and IL-4 (**d**) in serum, whole brain, prefrontal cortex (PFC), and hippocampus (HIP) in wild-type mice. Western blot analysis of PPARγ, p65, and p-p65 in the prefrontal cortex (**e**) and hippocampus (**f**) in C57 wild-type mice. Data are expressed as mean ± SEM: $^{*}P < 0.05$, $^{**}P < 0.01$, and $^{***}P < 0.001$ compared to control; $^{\#}P < 0.05$, $^{\#\#}P < 0.01$, and $^{\#\#\#}P < 0.001$ compared to DAC group

The GFAP-immunoreactive expression level in the prefrontal cortex and hippocampus was further detected with Western blot analysis. A significant group effect was observed in the prefrontal cortex ($F_{2,12} = 6.350$, $P = 0.013$), with a markedly lower level of GFAP-immunoreactive expression compared to the DAC group ($P = 0.049$) (Fig. 6c, d). There were no significant changes in the hippocampus.

Effects on Microglial M1/M2 Polarization in Brain Tissues

M1 and M2 phenotypes respectively represent pro- and anti-inflammatory activity of microglia in response to neuroinflammation [18]. Immunofluorescence was used to detect M1 (IL-6 and Iba-1) and M2 (Arg-1) markers in the prefrontal

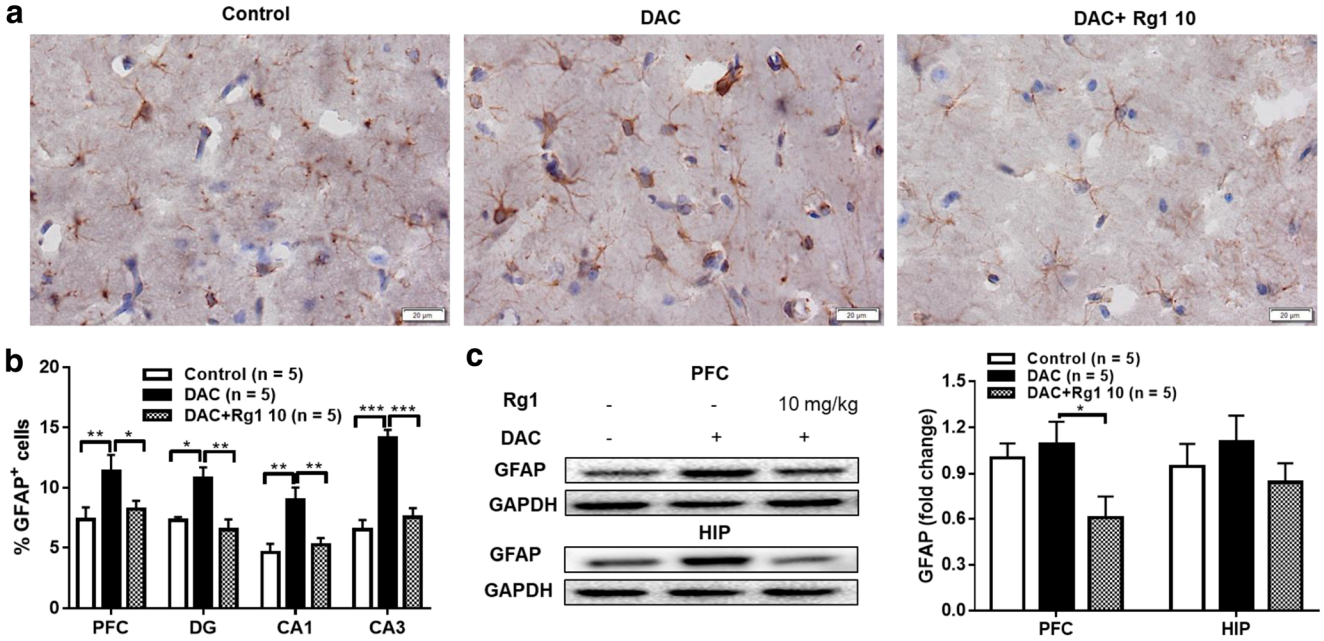

Fig. 6 Effects of 10 mg/kg Rg1 on the activation of astrocytes in DAC-treated mice. The representative morphology of astrocytes in hippocampus (**a**), the area of GFAP$^+$ cells in the related brain region (**b**), and Western blot analysis of GFAP in prefrontal cortex and hippocampus was analyzed (**c**). Data are expressed as mean ± SEM: $^*P < 0.05$, $^{**}P < 0.01$, and $^{***}P < 0.001$

cortex and the three hippocampal subregions, dentate gyrus, CA1, and CA3 (Fig. 7a–d). The appearance of microglia in the DAC group manifested as round and amoeboid-like shape with large perinuclear cytoplasm, dense and heterochromatic nucleus, in contrast to those with small and ovoid-shaped microglia in controlled and Rg1-treated mice. Significant group effects were present on microglial Iba-1$^+$ areas, IL-6$^+$/Iba-1$^+$ ratio, and Arg-1/Iba-1 ratio ($F_{2,12} \geq 35.220$, $P \leq 0.048$). The DAC group had a markedly greater percent of microglial Iba-1$^+$ areas and IL-6$^+$/Iba-1$^+$ ratio, but lower Arg-1/Iba-1 ratio in the prefrontal cortex and some or all hippocampal subregions than the other two groups ($P \leq 0.048$). These variables were not different between controlled and the Rg-1 treated mice.

Western blot analysis showed significant differences among the three groups in the expression of Arg-1 and IL-6 in the prefrontal cortex and hippocampus ($F_{2,12} \geq 16.270$, $P \leq 0.038$) (Fig. 7e–g). The DAC group displayed striking decreases in Arg-1 expression and increases in IL-6 expression in the prefrontal cortex and the hippocampus ($P \leq 0.038$). Rg1 co-treatment completely reversed DAC-induced alterations in prefrontal Arg-1 and IL-6, and hippocampal IL-6 expression ($P \leq 0.032$), without significant differences from controls.

Effects on Cultured Microglial and Neuronal Cells

The effects of DAC and Rg1 were re-examined in BV-2 microglial cells using immunofluorescence and Western blot (Fig. 8a–c). In immunofluorescence analysis on BV2 cells, one-way ANOVA revealed significant differences among five groups (control, LPS, DAC, 20 μM Rg1, and 40 μM Rg1) in Iba-1$^+$ areas of the cells ($F_{4,20} = 19.650$, $P = 0.004$) and counts of cells with nuclear p65-NFκB immunoreactivity ($F_{4,20} = 53.410$, $P < 0.0001$). Both toxin (LPS and DAC)-treated groups displayed striking increases in Iba-1$^+$ areas and significantly higher nuclear p65-NFκB$^+$ cell counts ($P < 0.000$) as compared to controls. Either two doses of Rg1 co-treatment completely suppressed toxin-induced increases of the Iba1$^+$ areas and decreased nuclear p65-NFκB$^+$ cell counts ($P \leq 0.0001$).

In Western blot analysis, significant group effects were observed on the expression of the three microglia-mediated neuroinflammatory biomarkers, p-p65-NFκB, IL-6, and TNF-α in BV2 cells ($F_{4,25} \geq 43.510$, $P \leq 0.011$) (Fig. 8d, e). Treatment with DAC and LPS robustly increased the expression of p-p65-NFκB, IL-6, and TNF-α as compared to controls ($P \leq 0.008$). Rg1 pretreatment completely suppressed toxin-induced increases in the expression of the three microglial markers ($P \leq 0.001$).

PC12 neuroblastic cells were treated with the media separately collected from the culture of BV2 cells. There was a significant difference in cell viability across the five groups ($F_{4,25} = 6.642$, $P \leq 0.001$) (Fig. 8f, g). LPS- and DAC-treated groups displayed an approximate 40% reduction in cell viability compared to controls ($P \leq 0.043$). Co-treatment with both doses of Rg1 completely protected against the toxin-induced loss of cell viability ($P \leq 0.0001$).

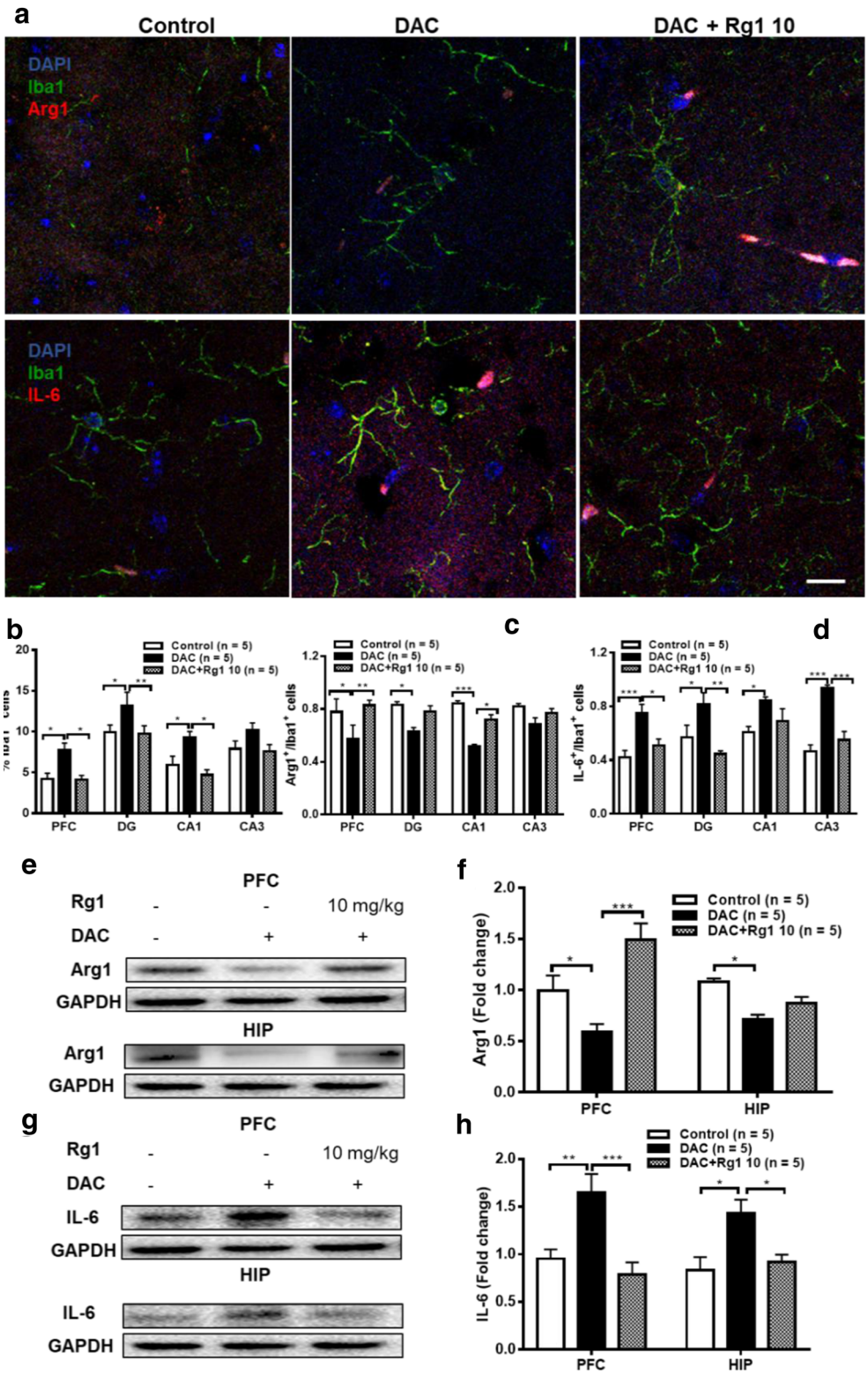

Fig. 7 Effects of 10 mg/kg Rg1 on the M2 and M1 phenotype of microglia in brain tissues. The representative morphology of microglia in hippocampus (**a**). The iba1$^+$ cells area (**b**) and the Arg1$^+$/Iba1$^+$ cells (**c**) and IL-6$^+$/Iba1$^+$ cells (**d**) were analyzed. The level of Arg1 and IL-6 also measured by Western blotting (**e**–**h**) (scale bar = 20 μm)

Discussion

Similar to our recent study [8], the present study once again validated the DAC regimen-produced mouse model of chemobrain, manifesting as a longer escape latency to the platform during the training trials, a shorter duration spent in, fewer entries, and longer first time into the targeted quadrant in the probe test as compared with untreated mice. Moreover, either DAC or Rg1 did not change locomotion and anxiety level, as evidenced by the lack of difference across

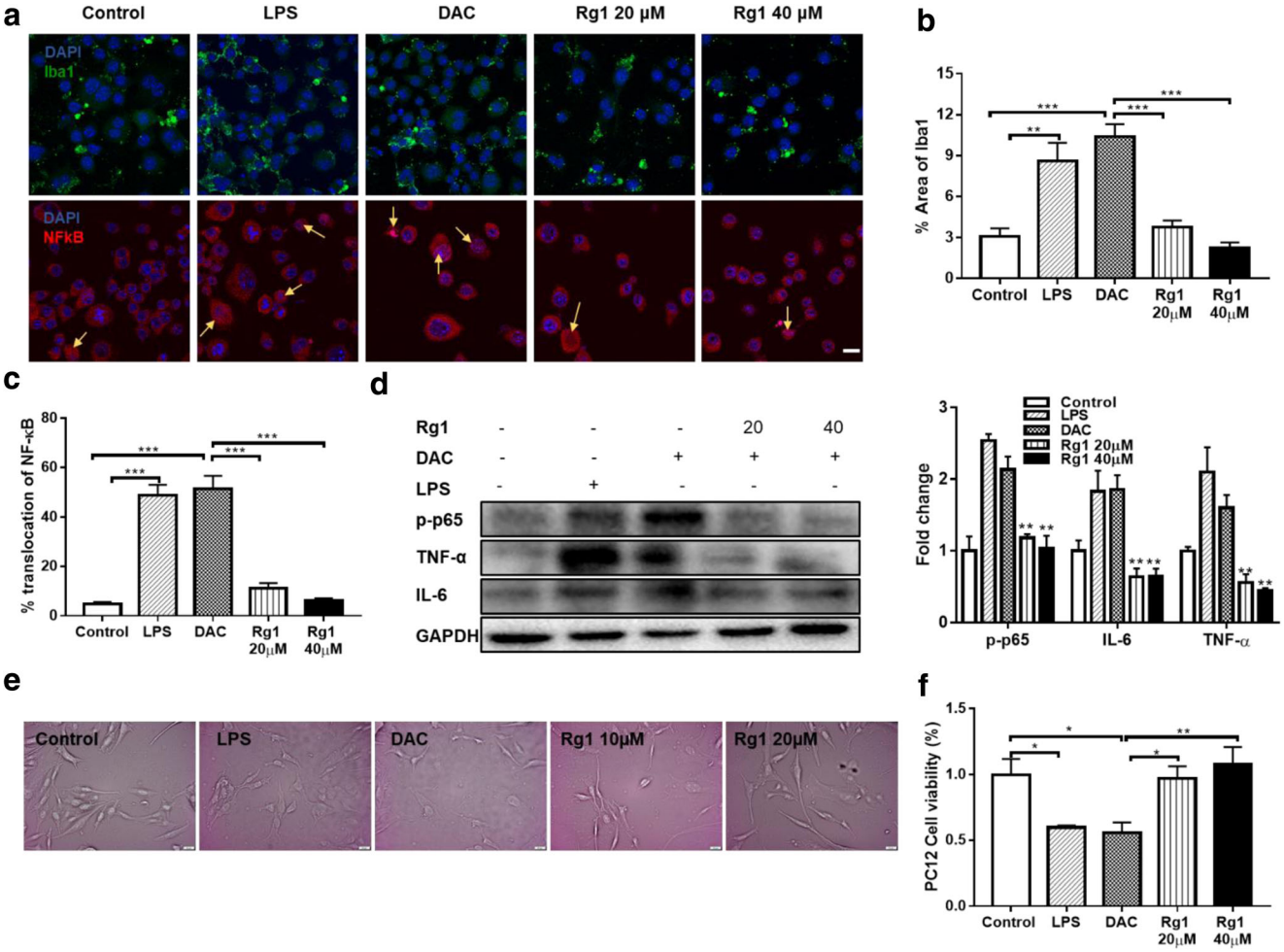

Fig. 8 The anti-neuroinflammation effects of rg1 were evaluated in BV2 cells and PC12 cells. The expression of Iba1 and NF-κB (**a**) were detected in BV2 cells. The area of Iba1$^+$ cells (**b**) and the translocation of NF-κB (**c**) was also analyzed. The neuroinflammation-related proteins in condition medium of BV2 were analyzed using western blotting (**d**, **e**). The cell viability (**g**) and morphology (**f**) of PC12 in BV2-conditioned medium was analyzed. The translocation of NF-κB are indicated with arrows (scale bar = 20 μm)

the four groups in the total distance traveled in the water maze and in the movement velocity in the open field; all of the groups spent similar amounts of time in the central zone and made similar numbers of entries into the central zone of the open field. These results clearly indicate that the effects of DAC and Rg1 on cognitive performance observed in the water maze is not due to locomotor abnormality or an elevated anxiety level, but a consequence of their specific effects on cognition processing.

This study showed the effects of Rg1, a ginseng-derived compound, in preventing chemobrain. Co-treatment with Rg1 at the high dose, but not the low dose, partially and even completely reversed DAC-induced decrease in latency to the hidden platform during the training trials and increases in duration spent in and number of entries into the targeted quadrant in the probe trial in water maze test. The nootropic effects of Rg1 have been widely observed in aged [19] and transgenic mice [20], animal models of cognitive impairment produced by various neurotoxins, including LPS [21], okadaic acid [22], scopolamine [23], and D-galactose [24].

On the other hand, our neuroimaging data revealed that chemotherapy caused remarkable decreases in prefrontal and hippocampal neuronal activity, and striking elimination and loss of neuronal dendritic spines in the prefrontal cortex. Similar neurotoxic effects were also observed in patients undergoing chemotherapy and animal models of chemobrain, exhibiting microstructural abnormality and aberrant neuroplasticity in distributed brain regions [25, 26]. In this study, Rg1 co-treatment, however, protected prefrontal and hippocampal neuronal activity and prefrontal neuronal spine plasticity from the neurotoxic effects of chemotherapy. Microdialysis has revealed that systemic administration of Rg1 could produce a distinct pharmacokinetic profile in the rat medial prefrontal cortex and hippocampus [27]. It thus appears that Rg1 may have specific targets on the prefrontal cortex and hippocampus, the two major brain regions directly involved in cognition processing [28]. This could at least

partially explain the anti-chemobrain and neuroimaging effects of Rg1 observed.

The protective effects of Rg1 on neuroplasticity were further confirmed in Western blot analysis of this study. The amino acid neurotransmitter receptors $GABA_AR$ and NMDAR1 which are widely distributed in interneurons of the brain, with their downstream mediators, BDNF/TrkB signaling pathway and intracellular Ca2+/CaMKII, play a crucial role in molecular regulation of neural plasticity and cognitive function [29, 30] and often serve as valid biomarkers for neuroplasticity [31]. In this study, while DAC regimen resulted in a dramatic overexpression of p-CaMKII and a broad suppression of the expression of the other five biomarkers examined in the prefrontal cortex and the hippocampus of the two strains of mice, the addition of Rg1, however, completely reversed the DAC's effects on all the six biomarkers in wild-type mice and on the majority of these biomarkers in the transgenic mice. These results clearly indicate a neuroprotective efficacy of Rg1 on neuroplasticity of glutamate and GABA interneuron network. Likewise, a large body of evidence confirms that Rg1 long-term treatment promoted electrophysiological and molecular synaptic plasticity of the hippocampus while improving learning and memory ability [11, 19, 32–36]. Together with the findings of this study, the promotion of hippocampal synaptic plasticity seems to be a key component in the mechanisms of Rg1's nootropic effects.

This study revealed that DAC not only induced overproduction of proinflammatory cytokines (IL-6 and TNF-α) and inhibited antiinflammatory cytokines (IL-10 and IL-4) in multiple serum, and whole and regional brain tissues in both strains of mice but also caused abnormal expression of multiple cytokine mediators of PPARγ/NF-κB pathways which play a crucial role in regulating neuroinflammation-related cytokine functions [37–39]. DAC reduced the expression of PPARγ, a member of the nuclear receptor family of transcription factors that inhibit inflammatory cytokine production [40], and increased NF-κB-p65 and IκBα phosphorylation. These results indicate that DAC exerts its neurotoxic effects largely via interference with the PPARγ/NF-κB signaling pathways. Either two doses of Rg1, however, broadly suppressed the overproduction of the proinflammatory cytokines and completely restored the anti-inflammatory cytokine levels. Rg1 also normalized DAC-induced abnormalities in the expression of brain cytokine mediators by restoring PPARγ activity and inhibiting NF-κB p65 and IκBα phosphorylation. The broad therapeutic effects of Rg1 have been found to be closely associated with its modulation of PPARγ/NF-κB signaling pathways in animal models of rheumatoid arthritis [39], cerebral ischemia [41, 42], and Alzheimer's disease [43]. The inhibition of cytokine-mediated inflammation via its upstream PPARγ/NF-κB signaling pathways may be a common mechanism responsible for the effects of Rg1 in attenuating various inflammatory conditions, including chemobrain.

As the primary source of proinflammatory cytokines in the central nervous system (CNS), the microglial system plays a pivotal role in the modulation of the neural response to inflammatory insults [44]. The activation of microglia can be polarized into the two phenotypes, M1 and M2, depending upon the local CNS microenvironments [45]. M1 activation leads to pro-inflammatory cytokine release, whereas M2 activation results in anti-inflammatory cytokine production [18]. In this study, DAC regimen activated astrocytes and microglial polarization, resulting in hyperplasia and overexpression of GFAP-labeled astrocytes and IL-6-labeled M1 phenotype microglia, but decreases in the expression of Arg-labeled M2 phenotype microglia in both brain tissues and cultured microglial cells. Like the neurotoxin LPS, DAC also produced neurotoxic effects by reducing PC12 neuroblastic cell viability, evoking the overexpression of the microglia-secreted inflammatory cytokines IL-6 and TNF-α, and increasing NF-κB-p65 translocation from the cytoplasm to the nucleus in BV2 microglial cells. However, as expected, Rg1 cotreatment inhibited astrocytic hyperplasia and microglial polarization from M2 to M1 phenotype. It also protected neuronal viability, inhibited IL-6 and TNF-α secretion of microglia, and blocked NF-κB-p65 nuclear translocation.

Together with the effects of Rg1 on the PPARγ/NF-κB signaling pathways, the anti-chemobrain effect of Rg1 observed in this study seems to be achieved mainly by inhibiting neuroinflammation via its broad modulation of microglia-mediated cytokine production and the related upstream mediators, protecting neuronal activity and promoting molecular and subcellular neuroplasticity in particular brain regions associated with cognition processing (Fig. 9). The most apparent targets for the anti-chemobrain effect of Rg1 seem to be upstream biomarkers of PPARγ/NF-κB signaling pathways and brain regional cytokines, in particular TNF-α, IL-6, IL-10, and IL-4. Clinical studies have revealed that the severity of chemotherapy-induced cognitive deterioration is associated with blood levels of IL-6, IL-4, and TNF-α in cancer patients [46–48]. Whether Rg1 could modulate peripheral cytokines in parallel with its improvement on chemobrain deserves further investigation in patients. This study also suggests that Rg1 may have the therapeutic potential for neuroinflammation-associated brain disorders in addition to cognitive impairment [19–24]. Indeed, there have been a large number of studies that have demonstrated protective effects of Rg1 against cerebral ischemic injury [41], major depression [49, 50], Parkinson's disease [51, 52], and post-traumatic stress disorder (PTSD) [53] in animal models. These effects of Rg1 share, to a greater or lesser extent, similar mechanisms as revealed in this study.

As Rg1 is a major component existing in various ginseng products which have been widely used in the treatment of

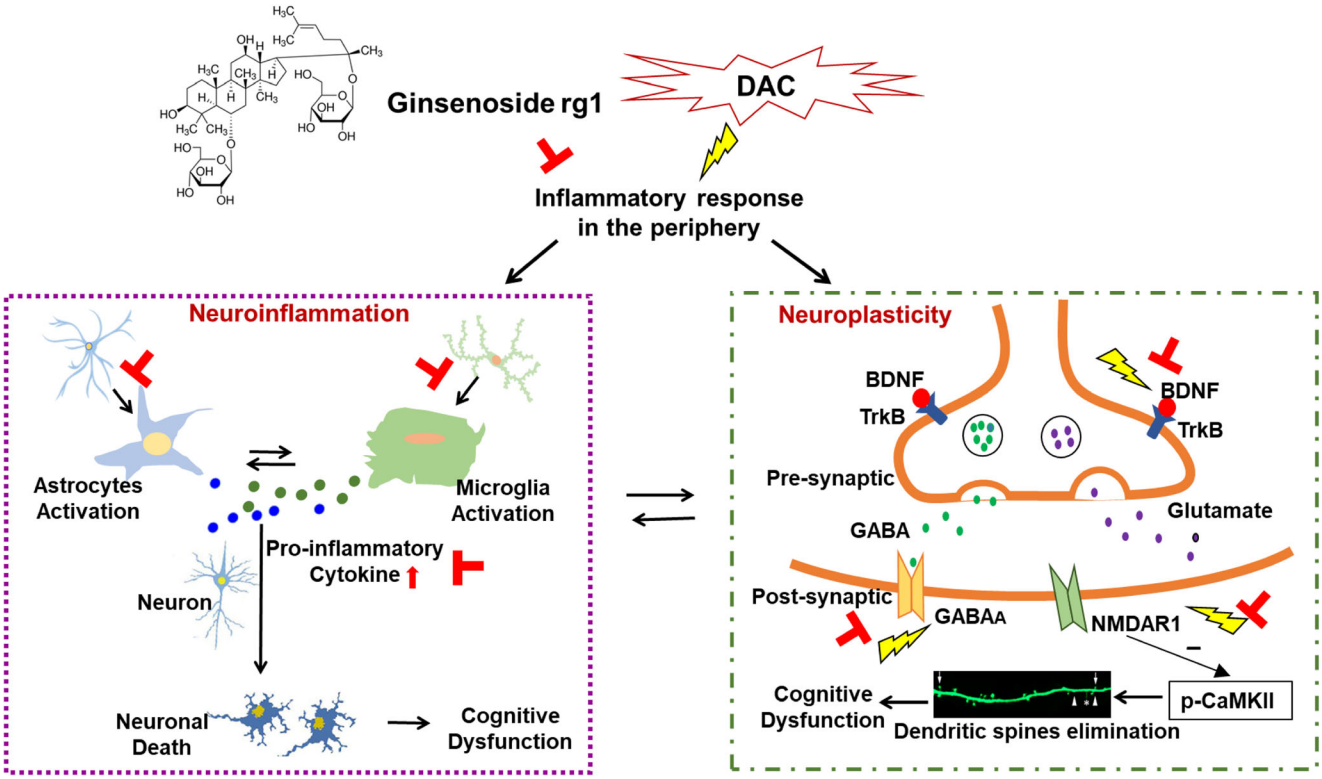

Fig. 9 Putative mechanisms of the preventive effects of Rg1 against chemobrain induced by DAC

chemotherapy-induced side effects in cancer patients [54], including breast cancer patients [55], the present study provides compelling evidence in support of the use of ginseng products as chemopreventive agents. An effective dose of 10 mg/kg/day of Rg1 used in mice of this study was equivalent to approximately 6 mg/day used for humans [56]. Ginseng is safe and tolerable at the recommended dose of 1–2 g of dry ginseng root or 200–600 mg of standardized ginseng extracts per day [57]. This recommended dose may be also valid for the prevention of chemobrain, as per gram of dry ginseng root contains approximately 3–5 mg Rg1 [58].

Several limitations of this study should be noted. First, this study only explored the acute effects, but did not evaluate chronic effects of chemotherapy on cognitive behavior. Whether similar cognitive impairment and nootropic effects of Rg1 also could be observed in long-term follow-up of chemotherapy needs further investigation. In addition, this study did not provide causal relationship and any underlying molecular mechanisms. Second, we detected the combination chemotherapy regimen, rather than single chemotherapeutic agents. Individual agents that might exert a major effect in inducing chemobrain could not be identified. Finally, we did not examine hippocampal neuronal dendritic spines in the transgenic mice due to methodological limitations [15, 16]. Despite this, cytokine measurement and immunodetection that showed similar results in the two strains of mice provide supplementary evidence to elucidate alterations in hippocampal plasticity.

Acknowledgements This study was supported by General Research Fund (GRF) of Research Grant Council of HKSAR (17115017 for Z.-J.Z.).

Compliance with Ethical Standards

Conflict of Interest Statement All authors have no conflicts of interest with this work.

Publisher's Note Springer Nature remains neutral with regard to jurisdictional claims in published maps and institutional affiliations.

References

1. Wefel JS, Schagen SB (2012) Chemotherapy-related cognitive dysfunction. Curr Neurol Neurosci Rep 12(3):267–275. https://doi.org/10.1007/s11910-012-0264-9
2. Deprez S, Amant F, Smeets A, Peeters R, Leemans A, Van Hecke W, Verhoeven JS, Christiaens MR et al (2012) Longitudinal assessment of chemotherapy-induced structural changes in cerebral white matter and its correlation with impaired cognitive functioning. J Clin Oncol Off J Am Soc Clin Oncol 30(3):274–281. https://doi.org/10.1200/jco.2011.36.8571
3. Taillibert S, Le Rhun E, Chamberlain MC (2016) Chemotherapy-related neurotoxicity. Curr Neurol Neurosci Rep 16(9):81. https://doi.org/10.1007/s11910-016-0686-x

4. Yao C, Bernstein LJ, Rich JB (2017) Executive functioning impairment in women treated with chemotherapy for breast cancer: a systematic review. Breast Cancer Res Treat 166(1):15–28. https://doi.org/10.1007/s10549-017-4376-4
5. Wang XM, Walitt B, Saligan L, Tiwari AF, Cheung CW, Zhang ZJ (2015) Chemobrain: a critical review and causal hypothesis of link between cytokines and epigenetic reprogramming associated with chemotherapy. Cytokine 72(1):86–96. https://doi.org/10.1016/j.cyto.2014.12.006
6. Tangpong J, Cole MP, Sultana R, Joshi G, Estus S, Vore M, St Clair W, Ratanachaiyavong S et al (2006) Adriamycin-induced, TNF-alpha-mediated central nervous system toxicity. Neurobiol Dis 23(1):127–139. https://doi.org/10.1016/j.nbd.2006.02.013
7. Cheung YT, Ng T, Shwe M, Ho HK, Foo KM, Cham MT, Lee JA, Fan G et al (2015) Association of proinflammatory cytokines and chemotherapy-associated cognitive impairment in breast cancer patients: a multi-centered, prospective, cohort study. Annals of oncology : Official journal of the European society for. Med Oncol 26(7):1446–1451. https://doi.org/10.1093/annonc/mdv206
8. Shi DD, Dong CM, Ho LC, Lam CTW, Zhou XD, Wu EX, Zhou ZJ, Wang XM et al (2018) Resveratrol, a natural polyphenol, prevents chemotherapy-induced cognitive impairment: involvement of cytokine modulation and neuroprotection. Neurobiol Dis 114:164–173. https://doi.org/10.1016/j.nbd.2018.03.006
9. Gao Y, Chu S, Li J, Li J, Zhang Z, Xia C, Heng Y, Zhang M et al (2015) Anti-inflammatory function of ginsenoside Rg1 on alcoholic hepatitis through glucocorticoid receptor related nuclear factor-kappa B pathway. J Ethnopharmacol 173:231–240. https://doi.org/10.1016/j.jep.2015.07.020
10. Gao Y, Chu S, Zhang Z, Chen N (2017) Hepataprotective effects of ginsenoside Rg1—a review. J Ethnopharmacol 206:178–183. https://doi.org/10.1016/j.jep.2017.04.012
11. Li F, Wu X, Li J, Niu Q (2016) Ginsenoside Rg1 ameliorates hippocampal long-term potentiation and memory in an Alzheimer's disease model. Mol Med Rep 13(6):4904–4910. https://doi.org/10.3892/mmr.2016.5103
12. Zhang X, Wang J, Xing Y, Gong L, Li H, Wu Z, Li Y, Wang J et al (2012) Effects of ginsenoside Rg1 or 17beta-estradiol on a cognitively impaired, ovariectomized rat model of Alzheimer's disease. Neuroscience 220:191–200. https://doi.org/10.1016/j.neuroscience.2012.06.027
13. Au HJ, Golmohammadi K, Younis T, Verma S, Chia S, Fassbender K, Jacobs P (2009) Cost-effectiveness analysis of adjuvant docetaxel, doxorubicin, and cyclophosphamide (TAC) for node-positive breast cancer: modeling the downstream effects. Breast Cancer Res Treat 114(3):579–587. https://doi.org/10.1007/s10549-008-0034-1
14. Mancuso JJ, Chen Y, Li X, Xue Z, Wong ST (2013) Methods of dendritic spine detection: from Golgi to high-resolution optical imaging. Neuroscience 251:129–140. https://doi.org/10.1016/j.neuroscience.2012.04.010
15. Sau Wan Lai C (2014) Intravital imaging of dendritic spine plasticity. Intravital 3(3):e944439. https://doi.org/10.4161/21659087.2014.984504
16. Lai CS, Franke TF, Gan WB (2012) Opposite effects of fear conditioning and extinction on dendritic spine remodelling. Nature 483(7387):87–91. https://doi.org/10.1038/nature10792
17. Stansley B, Post J, Hensley K (2012) A comparative review of cell culture systems for the study of microglial biology in Alzheimer's disease. J Neuroinflammation 9:115. https://doi.org/10.1186/1742-2094-9-115
18. Franco R, Fernandez-Suarez D (2015) Alternatively activated microglia and macrophages in the central nervous system. Prog Neurobiol 131:65–86. https://doi.org/10.1016/j.pneurobio.2015.05.003
19. Yang L, Zhang J, Zheng K, Shen H, Chen X (2014) Long-term ginsenoside Rg1 supplementation improves age-related cognitive decline by promoting synaptic plasticity associated protein expression in C57BL/6J mice. J Gerontol A Biol Sci Med Sci 69(3):282–294. https://doi.org/10.1093/gerona/glt091
20. Fang F, Chen X, Huang T, Lue LF, Luddy JS, Yan SS (2012) Multi-faced neuroprotective effects of ginsenoside Rg1 in an Alzheimer mouse model. Biochim Biophys Acta 1822(2):286–292. https://doi.org/10.1016/j.bbadis.2011.10.004
21. Jin Y, Peng J, Wang X, Zhang D, Wang T (2017) Ameliorative effect of ginsenoside Rg1 on lipopolysaccharide-induced cognitive impairment: role of cholinergic system. Neurochem Res 42(5):1299–1307. https://doi.org/10.1007/s11064-016-2171-y
22. Song XY, Hu JF, Chu SF, Zhang Z, Xu S, Yuan YH, Han N, Liu Y et al (2013) Ginsenoside Rg1 attenuates okadaic acid induced spatial memory impairment by the GSK3beta/tau signaling pathway and the Abeta formation prevention in rats. Eur J Pharmacol 710(1–3):29–38. https://doi.org/10.1016/j.ejphar.2013.03.051
23. Wang Q, Sun LH, Jia W, Liu XM, Dang HX, Mai WL, Wang N, Steinmetz A et al (2010) Comparison of ginsenosides Rg1 and Rb1 for their effects on improving scopolamine-induced learning and memory impairment in mice. Phytother Res 24(12):1748–1754. https://doi.org/10.1002/ptr.3130
24. Zhu J, Mu X, Zeng J, Xu C, Liu J, Zhang M, Li C, Chen J et al (2014) Ginsenoside Rg1 prevents cognitive impairment and hippocampus senescence in a rat model of D-galactose-induced aging. PLoS One 9(6):e101291. https://doi.org/10.1371/journal.pone.0101291
25. Simo M, Rifa-Ros X, Rodriguez-Fornells A, Bruna J (2013) Chemobrain: a systematic review of structural and functional neuroimaging studies. Neurosci Biobehav Rev 37(8):1311–1321. https://doi.org/10.1016/j.neubiorev.2013.04.015
26. Yang M, Moon C (2013) Neurotoxicity of cancer chemotherapy. Neural Regen Res 8(17):1606–1614. https://doi.org/10.3969/j.issn.1673-5374.2013.17.009
27. Xue W, Liu Y, Qi WY, Gao Y, Li M, Shi AX, Li KX (2016) Pharmacokinetics of ginsenoside Rg1 in rat medial prefrontal cortex, hippocampus, and lateral ventricle after subcutaneous administration. J Asian Nat Prod Res 18(6):587–595. https://doi.org/10.1080/10286020.2016.1177026
28. Rubin RD, Schwarb H, Lucas HD, Dulas MR, Cohen NJ (2017) Dynamic hippocampal and prefrontal contributions to memory processes and representations blur the boundaries of traditional cognitive domains. Brain Sci 7 (7). https://doi.org/10.3390/brainsci7070082
29. Mohler H (2007) Molecular regulation of cognitive functions and developmental plasticity: impact of GABAA receptors. J Neurochem 102(1):1–12. https://doi.org/10.1111/j.1471-4159.2007.04454.x
30. Sachser RM, Haubrich J, Lunardi PS, de Oliveira Alvares L (2017) Forgetting of what was once learned: exploring the role of postsynaptic ionotropic glutamate receptors on memory formation, maintenance, and decay. Neuropharmacology 112(Pt A):94–103. https://doi.org/10.1016/j.neuropharm.2016.07.015
31. Cervetto C, Taccola G (2008) GABAA and strychnine-sensitive glycine receptors modulate N-methyl-D-aspartate-evoked acetylcholine release from rat spinal motoneurons: a possible role in neuroprotection. Neuroscience 154(4):1517–1524. https://doi.org/10.1016/j.neuroscience.2008.04.066
32. Mook-Jung I, Hong HS, Boo JH, Lee KH, Yun SH, Cheong MY, Joo I, Huh K et al (2001) Ginsenoside Rb1 and Rg1 improve spatial learning and increase hippocampal synaptophysin level in mice. J Neurosci Res 63(6):509–515. https://doi.org/10.1002/jnr.1045
33. Qi D, Zhu Y, Wen L, Liu Q, Qiao H (2009) Ginsenoside Rg1 restores the impairment of learning induced by chronic morphine administration in rats. J Psychopharmacol 23(1):74–83. https://doi.org/10.1177/0269881107082950

34. Shi YQ, Huang TW, Chen LM, Pan XD, Zhang J, Zhu YG, Chen XC (2010) Ginsenoside Rg1 attenuates amyloid-beta content, regulates PKA/CREB activity, and improves cognitive performance in SAMP8 mice. J Alzheimers Dis 19(3):977–989. https://doi.org/10.3233/jad-2010-1296
35. Wang XY, Zhang JT (2001) Effects of ginsenoside Rg1 on synaptic plasticity of freely moving rats and its mechanism of action. Acta Pharmacol Sin 22(7):657–662
36. Zhu G, Wang Y, Li J, Wang J (2015) Chronic treatment with ginsenoside Rg1 promotes memory and hippocampal long-term potentiation in middle-aged mice. Neuroscience 292:81–89. https://doi.org/10.1016/j.neuroscience.2015.02.031
37. Omeragic A, Hoque MT, Choi UY, Bendayan R (2017) Peroxisome proliferator-activated receptor-gamma: potential molecular therapeutic target for HIV-1-associated brain inflammation. J Neuroinflammation 14(1):183. https://doi.org/10.1186/s12974-017-0957-8
38. Martin H (2010) Role of PPAR-gamma in inflammation. Prospects for therapeutic intervention by food components. Mutat Res 690(1–2):57–63
39. Zhang Y, Chen C, Jiang Y, Wang S, Wu X, Wang K (2017) PPARgamma coactivator-1alpha (PGC-1alpha) protects neuroblastoma cells against amyloid-beta (Abeta) induced cell death and neuroinflammation via NF-kappaB pathway. BMC Neurosci 18(1):69. https://doi.org/10.1186/s12868-017-0387-7
40. Clark RB, Bishop-Bailey D, Estrada-Hernandez T, Hla T, Puddington L, Padula SJ (2000) The nuclear receptor PPAR gamma and immunoregulation: PPAR gamma mediates inhibition of helper T cell responses. J Immunol 164(3):1364–1371
41. Li Y, Guan Y, Wang Y, Yu CL, Zhai FG, Guan LX (2017) Neuroprotective effect of the ginsenoside Rg1 on cerebral ischemic injury in vivo and in vitro is mediated by PPARgamma-regulated antioxidative and anti-inflammatory pathways. Evid Based Complement Alternat Med 2017:7842082. https://doi.org/10.1155/2017/7842082
42. Yang Y, Li X, Zhang L, Liu L, Jing G, Cai H (2015) Ginsenoside Rg1 suppressed inflammation and neuron apoptosis by activating PPARgamma/HO-1 in hippocampus in rat model of cerebral ischemia–reperfusion injury. Int J Clin Exp Pathol 8(3):2484–2494
43. Quan Q, Wang J, Li X, Wang Y (2013) Ginsenoside Rg1 decreases Abeta(1-42) level by upregulating PPARgamma and IDE expression in the hippocampus of a rat model of Alzheimer's disease. PLoS One 8(3):e59155. https://doi.org/10.1371/journal.pone.0059155
44. Streit WJ, Mrak RE, Griffin WS (2004) Microglia and neuroinflammation: a pathological perspective. J Neuroinflammation 1(1):14. https://doi.org/10.1186/1742-2094-1-14.
45. Peng H, Li H, Sheehy A, Cullen P, Allaire N, Scannevin RH (2016) Dimethyl fumarate alters microglia phenotype and protects neurons against proinflammatory toxic microenvironments. J Neuroimmunol 299:35–44. https://doi.org/10.1016/j.jneuroim.2016.08.006
46. Chae JW, Ng T, Yeo HL, Shwe M, Gan YX, Ho HK, Chan A (2016) Impact of TNF-alpha (rs1800629) and IL-6 (rs1800795) polymorphisms on cognitive impairment in Asian breast cancer patients. PLoS One 11:e0164204
47. Cheung YT, Ng T, Shwe M, Ho HK, Foo KM, Cham MT, Lee JA, Fan G et al (2015) Association of proinflammatory cytokines and chemotherapy-associated cognitive impairment in breast cancer patients: a multi-centered, prospective, cohort study. Ann Oncol 26:1446–1451
48. Ganz PA, Bower JE, Kwan L, Castellon SA, Silverman DH, Geist C, Breen EC, Irwin MR et al (2013) Does tumor necrosis factor-alpha (TNF-alpha) play a role in post-chemotherapy cerebral dysfunction? Brain Behav Immun 30(Suppl):S99–S108
49. Jiang B, Xiong Z, Yang J, Wang W, Wang Y, Hu ZL, Wang F, Chen JG (2012) Antidepressant-like effects of ginsenoside Rg1 are due to activation of the BDNF signalling pathway and neurogenesis in the hippocampus. Br J Pharmacol 166:1872–1887. https://doi.org/10.1111/j.1476-5381.2012.01902.x
50. Mou Z, Huang Q, Chu SF, Zhang MJ, Hu JF, Chen NH, Zhang JT (2017) Antidepressive effects of ginsenoside Rg1 via regulation of HPA and HPG axis. Biomed Pharmacother 92:962–971
51. Heng Y, Zhang QS, Mu Z, Hu JF, Yuan YH, Chen NH (2016) Ginsenoside Rg1 attenuates motor impairment and neuroinflammation in the MPTP-probenecid-induced parkinsonism mouse model by targeting α-synuclein abnormalities in the substantia nigra. Toxicol Lett 243:7–21
52. Sun XC, Ren XF, Chen L, Gao XQ, Xie JX, Chen WF (2016) Glucocorticoid receptor is involved in the neuroprotective effect of ginsenoside Rg1 against inflammation-induced dopaminergic neuronal degeneration in substantia nigra. J Steroid Biochem Mol Biol 155:94–103
53. Wang Z, Zhu K, Chen L, Ou Yang L, Huang Y, Zhao Y (2015) Preventive effects of ginsenoside Rg1 on post-traumatic stress disorder (PTSD)-like behavior in male C57/B6 mice. Neurosci Lett 605:24–28
54. Chen S, Wang Z, Huang Y, O'Barr SA, Wong RA, Yeung S, Chow MS (2014) Ginseng and anticancer drug combination to improve cancer chemotherapy: a critical review. Evid Based Complement Alternat Med 2014:168940. https://doi.org/10.1155/2014/168940
55. Cui Y, Shu XO, Gao YT, Cai H, Tao MH, Zheng W (2006) Association of ginseng use with survival and quality of life among breast cancer patients. Am J Epidemiol 163(7):645–653. https://doi.org/10.1093/aje/kwj087
56. Nair AB, Jacob S (2016) A simple practice guide for dose conversion between animals and human. J Basic Clin Pharm 7:27–31. https://doi.org/10.4103/0976-0105.177703
57. Helms S (2004) Cancer prevention and therapeutics: Panax ginseng. Altern Med Rev 9(3):259–274
58. Lee SM, Bae BS, Park HW, Ahn NG, Cho BG, Cho YL, Kwak YS (2015) Characterization of Korean red ginseng (Panax ginseng Meyer): history, preparation method, and chemical composition. J Ginseng Res 39(4):384–391. https://doi.org/10.1016/j.jgr.2015.04.009